Mon. Not. R. Astron. Soc. **000**, 000–000 (0000) Printed 21 May 2008 (MN LATEX style file v2.2)

The pulsating DA white dwarf star EC 14012−1446: results from four epochs of time-resolved photometry

G. Handler,[1] E. Romero-Colmenero,[2] J. L. Provencal,[3] K. Sanchawala,[4,5] M. A. Wood,[6] I. Silver,[6] W.-P. Chen [4]

[1] *Institut für Astronomie, Universität Wien, Türkenschanzstrasse 17, A-1180 Wien, Austria*
[2] *South African Astronomical Observatory, P.O. Box 9, Observatory 7935, South Africa*
[3] *Mt. Cuba Observatory & Dept. of Physics and Astronomy, University of Delaware, 223 Sharp Laboratory, Newark, DE 19716*
[4] *Graduate Institute of Astronomy, National Central University, Chung-Li 32054, Taiwan*
[5] *Physics Department, Birla Institute of Technology and Science, Pilani 333 031, India*
[6] *Dept. of Physics and Space Sciences & SARA Observatory, Florida Institute of Technology, Melbourne, FL 32901, USA*

Accepted 2007 July 17. Received 2007 August 13; in original form 2007 September 10

ABSTRACT

The pulsating DA white dwarfs are the coolest degenerate stars that undergo self-driven oscillations. Understanding their interior structure will help to understand the previous evolution of the star. To this end, we report the analysis of more than 200 h of time-resolved CCD photometry of the pulsating DA white dwarf star EC 14012−1446 acquired during four observing epochs in three different years, including a coordinated three-site campaign. A total of 19 independent frequencies in the star's light variations together with 148 combination signals up to fifth order could be detected. We are unable to obtain the period spacing of the normal modes and therefore a mass estimate of the star, but we infer a fairly short rotation period of 0.61 ± 0.03 d, assuming the rotationally split modes are $\ell = 1$. The pulsation modes of the star undergo amplitude and frequency variations, in the sense that modes with higher radial overtone show more pronounced variability and that amplitude changes are always accompanied by frequency variations. Most of the second-order combination frequencies detected have amplitudes that are a function of their parent mode amplitudes, but we found a few cases of possible resonantly excited modes. We point out the complications in the analysis and interpretation of data sets of pulsating white dwarfs that are affected by combination frequencies of the form $f_A + f_B - f_C$ intruding into the frequency range of the independent modes.

Key words: stars: variables: other – stars: white dwarfs – stars: oscillations – stars: individual: EC 14012−1446 – techniques: photometric

1 INTRODUCTION

White dwarf stars are the most common end point of stellar evolution. Almost all stars with masses below $8 M_\odot$ end their lives in the white dwarf stage, and most of them do so after being the central star of a Planetary Nebula. Once the central star has exhausted its nuclear fuel, it slowly cools and dims at nearly constant radius. As there is a definite low-temperature cutoff to the white dwarf luminosity function, it can be used to determine the age of the galactic disk (e.g. Winget et al. 1987, Richer et al. 2000) or stellar clusters (e.g. Hansen et al. 2007), although some theoretical uncertainties remain (see Fontaine, Brassard & Bergeron 2001 for a recent review).

While white dwarf stars cool, they cross three pulsational instability strips, i.e. regions where they exhibit self-driven nonradial oscillations. The hottest instability region contains pulsating PG 1159 stars (the GW Vir stars), the intermediate one consists of pulsating DB white dwarfs (the V777 Her stars), whereas pulsating DA stars (the ZZ Ceti stars) constitute the coolest white dwarf instability strip. If all white dwarfs showed self-excited pulsations as they pass through their instability domain, this would mean that the interior structure of the pulsators is representative of all white dwarfs. The ZZ Ceti instability strip is considered

to be pure by most authors (e.g. see Bergeron et al. 2004, Mukadam et al. 2004, Castanheira et al. 2007).

In any case, if a large number of oscillations can be detected and resolved in a given star, one can apply asteroseismic methods to it. In other words, the oscillations can be used to determine the interior structure of such stars. This is important for astrophysics in general, as the history of evolution of stars is engraved in the interiors of its end product, the white dwarf star. Fortunately, white dwarfs are well suited for asteroseismology because virtually complete pulsational mode spectra over a certain frequency interval were found in a number of cases (e.g. Winget et al. 1991, 1994), for instance for the prototype pulsating PG 1159 and DB white dwarf stars.

The pulsating DA white dwarfs have remained less accessible to this method. Their interior structure is somewhat more complicated due to their surface hydrogen layer and possible interior crystallization (e.g. Montgomery & Winget 1999). Their pulsational mode spectra are in general less dense than those of the pulsating PG 1159 and DB stars, and even so, some of the observed signals are difficult to be reconciled with theoretical models (e.g. Pech, Vauclair & Dolez 2006, or Castanheira et al. 2004).

Part of these difficulties may arise from combination frequencies, i.e. signals that may only reflect the Fourier decomposition of the non-sinusoidal light curve shapes and that do not correspond to normal mode oscillations, intruding into the frequency domain of the normal modes. Another potential problem is the occurrence of amplitude and frequency variations on short time scales (e.g. Handler et al. 2003), resulting in spurious peaks that complicate the identification of normal modes. On the other hand, the temporal variations of the pulsational spectra of some ZZ Ceti stars may make modes that are not permanently observable visible at some periods of observation. This fact was first recognized and taken advantage of by Kleinman et al. (1998).

Still, considerable progress in the understanding of ZZ Ceti star pulsation has been made recently. For instance, Kepler et al. (2005) pointed out how the C/O ratio in the core of these stars can be measured from their evolutionary period changes that reflect their cooling rate. Furthermore, based on the original idea by Brickhill (1992), Montgomery (2005) derived a method to constrain pulsational mode identifications from the light curve shapes of pulsating white dwarfs, and to recover the thermal response time scale of the convection zone, which depends on effective temperature.

Consequently, it is desirable to obtain extensive observations of multiperiodic ZZ Ceti stars, and to decipher their pulsational mode spectra. A good target for asteroseismic studies must be carefully chosen: in general, hot pulsating DA white dwarfs have few modes, low amplitudes and short periods, whereas the cooler pulsators have longer periods, higher amplitudes and more modes, but temporal variations in their pulsation spectra. The best choice may then lie in between: when observing pulsators in the centre of the ZZ Ceti instability strip, short and long periods, high amplitudes, as well as stable mode spectra may be present.

2 OBSERVATIONS AND REDUCTIONS

The ZZ Ceti star EC 14012−1446 was discovered to be a multiperiodic high-amplitude pulsator by Stobie et al. (1995), who found five independent and five combination frequencies in their data. As this object seemed well suited for asteroseismic purposes, we have obtained time-resolved CCD photometry of the star over four epochs distributed over three years. Three of the data sets were acquired at a single site, but one data set was obtained during a coordinated campaign involving three observatories well spread in geographical longitude.

The first measurements originated from the 0.75-m telescope at the South African Astronomical Observatory (SAAO) and were taken in April 2004. A high-speed CCD photometer (O'Donoghue 1995) was used in frame-transfer mode with integration times of 10 seconds. No filter was employed.

Two months later, we observed EC 14012−1446 with the 1.9-m telescope at the SAAO with the same photometer. Due to the smaller field of view, frame-transfer mode was not employed, but the integration time of 10 seconds was kept, resulting in one frame per 12 seconds, and again no photometric filter was inserted.

In the year 2005, we organized a multi-site campaign for the star, involving three observatories in South Africa, the United States and Taiwan. In this way, close-to uninterrupted measurements could be obtained during the central part of the campaign. The 1.0-m telescope at Lulin Observatory started the observations, which were taken as unfiltered 12-second integrations, resulting in one frame per 17 seconds. The 1.0-m telescope at SAAO came on line four nights afterwards, this time using a standard CCD with 21-second exposures and no filter, yielding one data frame every 30 seconds. Later during the same night, the 0.9-m telescope of the Southeastern Association for Research in Astronomy (SARA) located in Arizona joined the campaign, acquiring unfiltered measurements with 12-second exposures for one data point per 16 seconds.

Finally, in 2007, the 0.9-m telescope at the Cerro Tololo Interamerican Observatory (CTIO) was used to measure EC 14012−1446 again. These data were acquired through a S8612 red-cutoff filter. The integration time was 10 seconds, leading to a data rate of one frame per 30 seconds. The star was observed every second night of this run. An overview of all the observing runs is given in Table 1.

All measurements from the years 2004 and 2005 were reduced in the same way. First, standard IRAF[1] routines were used to correct the images for overscan, bias level (if needed), dark counts (if needed) and flat field. Photometry was carried out using the MOMF (Multi–Object Multi–Frame, Kjeldsen & Frandsen 1992) package. MOMF applies combined Point–Spread Function/Aperture photometry relative to an optimal sample of comparison stars, ensuring highest-quality differential light curves of the target.

The CTIO data from 2007 were also reduced with IRAF in the above-mentioned way, but photometry was carried out with a series of IRAF scripts employing aperture photom-

[1] IRAF, the Image Reduction and Analysis Facility, is written and supported by the IRAF programming group at the National Optical Astronomy Observatories (NOAO) in Tucson, Arizona.

Table 1. Overview of the observations. ΔT is the total time of monitoring, and Δf is the frequency resolution of the data set. For the multisite campaign, the frequency resolution of the combined data is quoted and marked with an asterisk.

Month/Year	Telescope	# nights	ΔT (hr)	Δf (μHz)
April 2004	SAAO 0.75-m	4	36.4	2.2
June 2004	SAAO 1.9-m	4	18.6	3.7
May 2005	Lulin 1.0-m	7	26.8	0.75*
May 2005	SAAO 1.0-m	8	50.9	0.75*
May 2005	SARA 0.9-m	5	30.5	0.75*
April 2007	CTIO 0.9-m	7	40.1	0.87
Total		35	203.3	

etry optimized for high-speed CCD data (Kanaan, Kepler & Winget 2002). The final output from these scripts again is a differential light curve of the target star. Tests showed that both of the CCD photometry programs employed by us yield results of comparable quality.

All differential light curves were visually inspected and data obtained during poor photometric conditions were removed. As EC 14012−1446 is substantially bluer than the nearby stars used as comparisons, some differential colour extinction present in the light curves was carefully removed with the Bouguer method (fitting a straight line to a plot of magnitude vs. air mass). No low-frequency filtering was performed to avoid affecting possible intrinsic long-period signals. Finally, as no periodicities shorter than 140 seconds were present in the light curves, some data were merged to speed up the computations to follow: the April 2004 data were co-added to 20-second bins, the June 2004 data to 24-second bins, the Lulin measurements from 2005 to 34-second bins and the SARA data from 2005 to 32-second bins. This procedure also ensured that the 2005 campaign data all have similar time sampling and therefore similar weight in frequency analyses.

Finally, all measurements were transformed to a common time base. We chose Terrestrial Time (TT) as our reference for measurements on the Earth's surface and applied a correction to account for the Earth's motion around the solar system's barycentre. As this barycentric correction varied by up to −1.7 s during single observing nights, we applied it point by point. Our final time base therefore is Barycentric Julian Ephemeris Date (BJED). The resulting time series was subjected to frequency analysis.

3 FREQUENCY ANALYSIS

The frequency analysis was mainly performed with the program `Period98` (Sperl 1998). This package applies single-frequency power spectrum analysis and simultaneous multi-frequency sine-wave fitting. It also includes advanced options such as the calculation of optimal light-curve fits for multi-periodic signals including harmonic and combination frequencies. Our analysis will require these features.

We began by computing the Fourier spectral window functions of all data sets, and show the results in Fig. 1. The multisite campaign (May 2005) resulted in a reasonably clean window, whereas the other data sets suffer from aliasing. The April 2004 window has strong sidelobes not only at the daily alias 11.6 μHz away from the correct frequency, but also at 2.8, 8.8 and 14.3 μHz, respectively. The June 2004 measurements have the poorest window function with low frequency resolution and strong diurnal aliases, and the April 2007 data suffer not only from daily aliasing, but also from spurious signals 5.2, 6.4, 16.9 and 18.0 μHz away from the correct frequency. This has to be kept in mind when carrying out a frequency search.

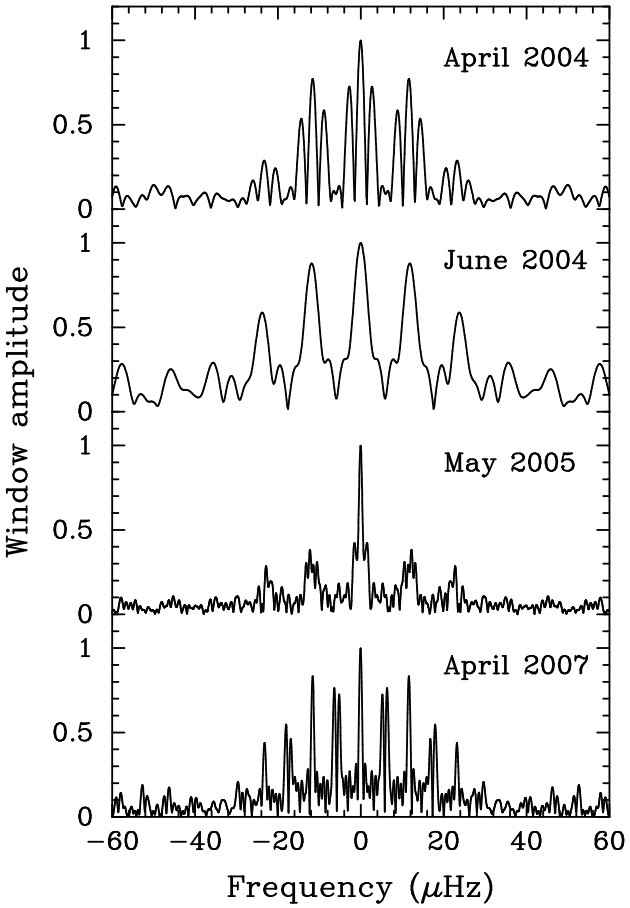

Figure 1. The spectral window functions of our data sets from the four different epochs.

We proceeded by computing the Fourier amplitude spectra of the individual data sets, which can be found on the right-hand side of Fig. 2. Both the light curves on the left-hand side of Fig. 2 as well as the amplitude spectra make it immediately obvious that the dominant time scale of the light variations of EC 14012−1446 increased and that the amplitudes of individual pulsational signals also changed over time.

Under these circumstances (individual data sets with time bases that are short compared to their separations, often complicated window functions, variable periods and amplitudes) it becomes clear that the frequency analysis will be difficult and that the data sets cannot be analysed jointly. We therefore used a different strategy: initiating the analysis with the apparently best data subset, and then using the experience gained for examining the other subsets.

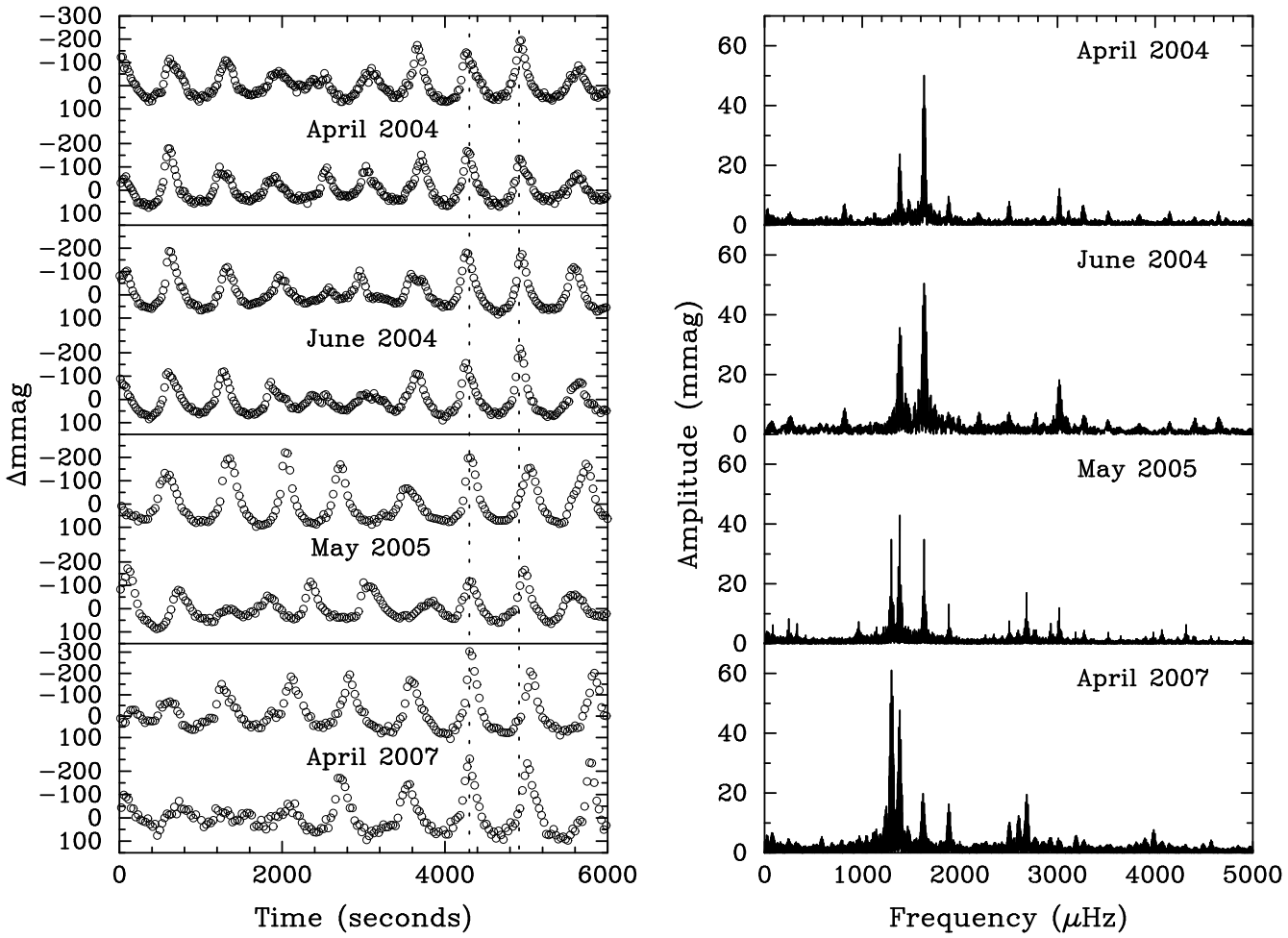

Figure 2. Some example light curves (left-hand side) and the amplitude spectra of our data sets from the four different epochs. The dotted vertical lines denote the average distance between consecutive light maxima in the April 2004 data; note the temporal increase of the "mean" variability period directly visible in the light curves.

3.1 The May 2005 multisite data

We started the analysis by computing Fourier amplitude spectra of the light curves, and then determined the frequencies of the strongest signals. These frequencies served as input parameters for a fit to the light curves that was optimized by nonlinear least squares sine-wave fitting implemented in `Period98`. In case of ambiguities due to aliasing, the frequency that yielded the lowest residuals between light curve and fit after optimization was chosen as input. As the next step, we prewhitened the fit from the light curve, computed the Fourier amplitude spectrum of the residuals and used it to search for further periodic signals.

After a few prewhitening steps it became clear that amplitude and/or frequency variations had occurred during the multisite campaign. This imposes severe complications on frequency analyses with Fourier algorithms, whose fundamental assumption is that the amplitudes and frequencies of the individual signals present are constant within the data set. We therefore decided to use only the central part of the data set for the purpose of frequency search. This core part of the run contained 69% of the campaign data, spanned 5.6 d, corresponding to a frequency resolution of 2.1 μHz and had a duty cycle of 53%.

Using only the central part of the run, we carried on with the prewhitening process as described above. Each signal detected during this procedure was checked whether or not it was a combination frequency, i.e. whether it corresponded to a harmonic, sum, or difference frequency of signals detected previously, within the frequency resolution of the data set (Table 1). If so, its frequency was fixed to the exact sum or difference of its parent signals within `Period98`. This procedure is valid here because the changes in the combination frequencies traced the changes in the parent modes within the accuracy of our data.

In some cases, particularly for possible combinations of higher order, ambiguities arose because more than one set of parent frequencies could be matched to a given combination within the resolution of the data set. We then chose these parent frequencies whose product of amplitudes was highest, and required that the parent frequencies must have higher amplitudes than the combination signal they generate.

Under these assumptions it is possible that the frequencies of some independent modes would be misidentified as combinations. However, we believe that disregarding a possi-

ble mode frequency is the safer choice compared to possibly accept some signals as real modes that are not.

We continued the analysis until no significant peak was left in the residual amplitude spectrum, adopting the signal-to-noise criterion by Breger et al. (1993, 1999). In brief, an independent signal must exceed an amplitude signal-to-noise of 4 to be accepted, whereas $S/N > 3.5$ is sufficient for combination signals. We refer to the two papers mentioned before for detailed discussions. In the end, 15 independent frequencies and 90 combination signals up to fifth order were detected.

3.2 The April 2004 data

Because of the long nightly time series acquired during our first observing run on the star (more than nine hours per night on average), this single-site data set is also well suited for frequency analyses. With the same procedures as described before, we detected 12 independent and 44 combination frequencies in this data set, with no evidence for amplitude and/or frequency variations throughout the observations.

3.3 The June 2004 data

Although acquired with the largest telescope we had available for this study, this data set is not ideal for frequency analysis. The spectral window function is complicated and the frequency resolution is poor (see Fig. 1). Only the strongest signals could be detected without ambiguity, and we had to resort to adopting frequencies determined from the April 2004 data to avoid aliasing problems when trying to reveal signals with poorer signal-to-noise. Our frequency solution for this data set containing 10 independent and 27 combination frequencies is probably incomplete. On the other hand, we believe that we have resisted the temptation to over-interpret this data set.

3.4 The April 2007 data

These measurements have the best formal frequency resolution, but due to their sampling the spectral window is complicated. Still, we could determine a large number of the signals in the light curves independently, and only in a few cases we had to adopt frequencies known from analyses of the other data sets. Amplitude and/or frequency variations likely occurred during these observations as well, but not on a scale severely hampering our analysis. Finally, we arrived at 11 independent and 40 combination frequencies for this data set.

3.5 Putting it all together

After the analyses of the individual data sets were completed, the results were merged and the frequency solutions were compared. We list all 19 independent frequencies in our light curves in Table 2, all 52 first-order combination frequencies in Table 3, all 60 third-order combination frequencies in Table 4, and all 29 fourth-order combination frequencies together with the 7 fifth-order combinations in Table 5.

4 DISCUSSION

4.1 The independent frequencies

As can be seen in Table 2, some, but not all of the independent frequencies are consistently present in all data sets. Some are singlets, and some show (regular) frequency splittings. This requires individual discussions of all these signals or signal groups. Again, we start with the simplest cases and move on to the more difficult ones, choosing to proceed from the highest frequencies to the lowest.

The signal at 2504 μHz is well-behaved. It is present throughout all data sets, with its frequency and amplitude roughly staying constant, and it shows no splittings. It is the best candidate to search for possible evolutionary period changes, but our data are not sufficient to reach a definite conclusion in this respect. We note, and caution, that in the discovery data by Stobie et al. (1995) this signal had an amplitude 60% higher than in our measurements.

The 1887 μHz variation is reasonably stable as well. However, in most data sets it had a companion near 1881 μHz, which is identified with a third-order combination frequency. The amplitude of the 1887 μHz signal increased with time. This finding must be taken with caution because there is no information about the star's behaviour between the different data sets. This signal also showed a higher amplitude in the Stobie et al. (1995) data than in any of our data sets.

A frequency triplet centred at 1633 μHz is present in all data sets. This triplet is always equally spaced within the errors, but the amount of the splitting varied: from 10.06 μHz in April 2004 to 9.73 μHz in June 2004, to 9.59 μHz in May 2005 and to 10.44 μHz in April 2007. Given the amount by which this splitting changes and the observational errors, this variation is probably intrinsic to the star.

An independent frequency at 1474 μHz is also detected in each individual data set. In May 2005 it was a singlet, in June 2004 and April 2007 it was accompanied by another independent frequency lower by 10.8 and 9.1 μHz, respectively, and in April 2004 it even was the centre of a triplet split by 9.98 μHz. Within the errors, this splitting is consistent with the separation of the triplet around 1633 μHz in the same period of observation (April 2004).

A strong signal at 1385 μHz is present in all data sets. In April and June 2004 it had a companion at a frequency 9.97 and 10.60 μHz lower, respectively. However, in April 2007 the 1385 μHz signal was the centre of an equally spaced frequency triplet separated by 14.48 μHz. In May 2005, the situation is even more difficult: we found complicated structure in this frequency region, with altogether six peaks and with the presence of two triplets centred on 1385 μHz with both the ≈ 10 and ≈ 14 μHz splittings. We note that the separation of some of the neighbouring signals is close to the resolution of our data set ($1.5/\Delta T$, where T is the time base of the data, Loumos & Deeming 1978), but these signals remain at the same frequencies when the full campaign data set is considered.

At the two later observing epochs, a strong signal at 1300 μHz emerged. It was the strongest peak the amplitude spectrum in April 2007 as a singlet, and in May 2005 it had two lower-frequency companions separated by 3.3 and 9.7 μHz, respectively. There was no trace of it in our mea-

Table 2. Independent frequencies in our light curves of EC 14012−1446. The formal errors in the amplitudes are ±0.4 mmag for April 2004, ±0.5 mmag for June 2004, ±0.3 mmag for May 2005 and ±0.5 mmag for April 2007

	April 2004		June 2004		May 2005		April 2007	
ID	Freq. (μHz)	Ampl. (mmag)	Freq. (μHz)	Ampl. (mmag)	Freq. (μHz)	Ampl. (mmag)	Freq. (μHz)	Ampl. (mmag)
f_1	821.26 ± 0.06	7.1	821.52 ± 0.13	7.8				
f_2	1132.89 ± 0.14	2.9						
f_3					1289.28 ± 0.06	5.3		
f_4					1295.73 ± 0.04	8.7		
f_5					1299.00 ± 0.01	39.8	1300.62 ± 0.01	63.6
f_6					1371.89 ± 0.04	9.1	1370.89 ± 0.01	20.0
f_7	1375.53 ± 0.08	5.5	1375.02 ± 0.15	6.9	1375.60 ± 0.07	4.7		
f_8					1381.97 ± 0.03	9.6		
f_9	1385.50 ± 0.02	24.4	1385.62 ± 0.03	35.1	1384.84 ± 0.01	40.6	1385.32 ± 0.01	44.1
f_{10}					1394.91 ± 0.04	7.3		
f_{11}					1398.29 ± 0.03	10.9	1399.84 ± 0.02	13.6
f_{12}	1464.17 ± 0.13	3.2	1464.17 ± 0.15	6.8			1463.95 ± 0.04	6.4
f_{13}	1474.12 ± 0.04	9.3	1474.95 ± 0.11	9.1	1473.02 ± 0.06	5.6	1473.04 ± 0.04	6.3
f_{14}	1484.13 ± 0.16	2.6						
f_{15}	1623.28 ± 0.04	11.2	1623.51 ± 0.11	9.0	1623.86 ± 0.03	10.5	1623.20 ± 0.01	18.6
f_{16}	1633.36 ± 0.01	48.1	1633.60 ± 0.02	48.3	1633.71 ± 0.01	33.5	1633.69 ± 0.05	4.7
f_{17}	1643.40 ± 0.03	14.2	1642.96 ± 0.07	13.6	1643.03 ± 0.05	7.0	1644.08 ± 0.06	4.1
f_{18}	1887.47 ± 0.05	8.9	1887.79 ± 0.11	9.3	1887.34 ± 0.03	12.3	1887.59 ± 0.02	15.2
f_{19}	2504.86 ± 0.05	8.7	2504.98 ± 0.12	8.1	2504.97 ± 0.05	6.8	2504.65 ± 0.03	8.6

surements from 2004, and it was not detected by Stobie et al. (1995).

The two lowest-frequency independent variations in our light curves were only present during (part of) 2004: a singlet at 1133 μHz in April, and another singlet at 821 μHz in both observing periods in 2004. We note that although numerically consistent in June 2004, an interpretation of f_1 as the subharmonic of f_{17} generated a poor fit to the data and was therefore rejected.

Stobie et al. (1995) reported an additional independent frequency of 1067 μHz in their discovery data. However, it was only present in their first night of observation, and we cannot confirm its presence in any of our data sets. As we do not have the data by Stobie et al. (1995) at our disposal, we will not discuss this signal any further.

4.1.1 Short-term amplitude and frequency variations

As noted before, we had to concentrate our frequency analysis of the May 2005 multisite photometry on the central part with the highest duty cycle because amplitude variations had occurred during the observations. After prewhitening the multifrequency solution listed in Tables 2 − 5 from these data, we still find residual mounds of amplitude left around most of the independent frequencies, most notably in the region with the most complicated structure around 1385 μHz.

This raises the suspicion that at least some of the signals in this frequency domain are artefacts due to amplitude and/or frequency variability. However, tests to check this hypothesis remained inconclusive. Consequently, it is not clear whether or not all the signals around 1385 μHz (Table 2) indeed correspond to normal mode frequencies.

We examined the occurrence of amplitude and frequency variations in the May 2005 data. We used the full data set for this purpose, and selected six independent signals, either singlets or the strongest multiplet components. First, all but these signals were prewhitened from the light curves, using Tables 2 − 5 as input and assuming constant amplitude and phase for all variations. We subdivided the residual light curves into sections long enough to avoid beating within the six independent signals under consideration and computed the amplitudes and phases for each. These are represented in graphical form in Fig. 3.

It is hard to say something quantitatively about the amplitude and frequency changes (which would require an even higher observational duty cycle), but we can make some qualitative statements.

- All independent signals do show amplitude and frequency modulation, with the possible exception of f_{19}.
- In general, signals at lower frequency (and therefore higher radial overtone) show more erratic behaviour.
- Amplitude variations are always accompanied by phase (frequency) variations. Whenever the amplitude is constant, the frequency is also constant.

Figure 3 also confirms that the amplitudes and phases of the variations remained constant during the central part of the observations, validating the most important assumption of the frequency analysis in Sect. 3.1.

Finally, we point out the interesting behaviour of signal f_{13} (top right panels in Fig. 3): it showed two phase "jumps" of $\approx \pi$ rad, at the beginning and the end of the observations. This might be an effect of beating between closely spaced signals. The amplitude spectrum of the full data set indeed shows two peaks of similar amplitude spaced by 1.3 μHz at this frequency. However, such a close frequency doublet is not present at a significant level in the measurements from 2007 that would also have the time base to resolve it.

Table 3. Second-order combination frequencies in our light curves of EC 14012−1446

	April 2004		June 2004		May 2005		April 2007	
ID	Freq. (μHz)	Ampl. (mmag)	Freq. (μHz)	Ampl. (mmag)	Freq. (μHz)	Ampl. (mmag)	Freq. (μHz)	Ampl. (mmag)
$f_6 - f_5$							70.27	3.9
$f_9 - f_5$					85.83	5.9	84.69	6.7
$f_{12} - f_5$							163.33	3.1
$f_{16} - f_9$	247.86	2.8	247.98	4.9	248.87	7.1		
$f_{15} - f_6$							252.31	3.9
$f_{18} - f_{16}$	254.12	3.6						
$f_{17} - f_7$			267.94	5.9				
$f_{15} - f_5$							322.58	2.9
$f_{16} - f_5$					334.71	6.0		
$f_{17} - f_5$							343.45	3.0
$f_{18} - f_9$					502.50	1.8	502.27	2.5
$f_{18} - f_5$					588.34	1.9	586.97	5.0
$f_{19} - f_{15}$							881.44	3.5
$f_{19} - f_6$							1133.75	5.2
$f_1 + f_7$	2196.79	3.3	2196.55	5.4				
$f_1 + f_9$	2206.76	2.4						
$f_1 + f_{13}$	2295.39	1.6	2296.48	2.7				
$f_1 + f_{16}$	2454.62	3.0	2455.13	4.1				
$2f_5$					2598.00	4.6	2601.25	12.8
$f_5 + f_6$							2671.52	7.5
$f_5 + f_9$					2683.84	17.3	2685.94	18.8
$f_5 + f_{10}$					2693.91	3.1		
$f_5 + f_{11}$					2697.29	2.9	2700.47	5.6
$f_6 + f_9$					2756.72	3.7	2756.21	4.6
$f_5 + f_{12}$							2764.58	3.8
$2f_9$	2770.99	1.7	2771.25	5.8	2769.67	2.3	2770.64	3.7
$f_5 + f_{13}$					2772.02	3.0		
$f_9 + f_{11}$					2783.12	1.6	2785.16	3.0
$f_6 + f_{13}$					2844.91	2.0		
$f_9 + f_{13}$	2859.62	2.8	2860.58	2.1				
$f_5 + f_{15}$							2923.83	4.7
$f_4 + f_{16}$					2929.43	2.0		
$f_5 + f_{16}$					2932.71	8.5		
$f_6 + f_{16}$					3005.60	3.7		
$f_9 + f_{15}$					3008.70	1.8	3008.52	4.8
$f_9 + f_{16}$	3018.85	12.3	3019.23	15.7	3018.54	10.4		
$f_{11} + f_{15}$					3022.15	3.3	3023.05	3.7
$f_9 + f_{17}$	3028.89	3.5	3028.58	5.4	3027.86	2.0		
$f_{13} + f_{16}$	3107.48	5.0	3108.56	4.1				
$f_{13} + f_{17}$	3117.52	1.6						
$f_5 + f_{18}$					3186.34	3.4	3188.22	5.0
$f_{15} + f_{16}$	3256.63	3.1	3257.12	3.5				
$2f_{16}$	3266.71	6.2	3267.21	6.2	3267.42	2.8		
$f_9 + f_{18}$	3272.97	1.9			3272.18	3.2	3272.91	4.4
$f_{16} + f_{17}$	3276.75	4.0	3276.56	3.7				
$f_{16} + f_{18}$	3520.83	4.2	3521.39	4.6	3521.05	4.2		
$f_5 + f_{19}$							3805.27	2.8
$f_9 + f_{19}$	3890.36	1.7						
$f_{11} + f_{19}$					3903.26	2.1	3904.49	3.1
$f_{16} + f_{19}$	4138.22	2.0	4138.58	2.8				
$f_{17} + f_{19}$	4148.26	4.0	4147.94	3.4				
$f_{18} + f_{19}$					4392.31	1.0		

4.2 The second-order combination frequencies

The combination frequencies appearing in Fourier analysis of the light curves of pulsating white dwarf stars are most commonly interpreted as nonlinear distortions, most likely originating in their surface convection zones (Brickhill 1992). However, an alternative interpretation is resonantly coupled modes (Dziembowski 1982). These two hypotheses are often difficult to separate, but as a general rule of thumb resonantly excited modes should have considerably larger amplitudes compared to signals that reflect light-curve distortions.

Table 4. Third-order combination frequencies in our light curves of EC 14012−1446

	April 2004		June 2004		May 2005		April 2007	
ID	Freq. (μHz)	Ampl. (mmag)	Freq. (μHz)	Ampl. (mmag)	Freq. (μHz)	Ampl. (mmag)	Freq. (μHz)	Ampl. (mmag)
$2f_5 - f_{17}$							957.17	3.4
$2f_4 - f_{16}$					957.74	2.2		
$f_4 + f_5 - f_{16}$					961.02	4.3		
$2f_5 - f_{16}$					964.30	8.9		
$2f_5 - f_{15}$					974.14	3.8		
$f_5 + f_9 - f_{16}$					1050.13	3.3		
$f_5 + f_9 - f_{15}$					1059.98	2.5		
$2f_9 - f_{17}$					1126.64	2.7		
$2f_9 - f_{16}$					1135.96	3.5		
$2f_5 - f_{12}$							1137.30	4.8
$2f_9 - f_{15}$					1145.81	3.2		
$f_5 + f_6 - f_{12}$							1207.57	4.4
$f_4 + f_5 - f_9$					1209.89	2.0		
$2f_5 - f_9$					1213.17	2.3	1215.93	4.9
$2f_5 - f_6$							1230.36	8.9
$f_5 + f_9 - f_{11}$					1285.55	6.6		
$f_5 + f_{10} - f_9$					1309.07	6.1		
$f_5 + f_9 - f_6$							1315.05	4.5
$2f_{16} - f_{18}$	1379.24	3.1						
$2f_9 - f_5$					1470.67	3.6		
$f_9 + f_{16} - f_{13}$					1545.53	2.1		
$f_5 + f_{16} - f_9$					1547.88	2.7		
$f_9 + f_{17} - f_{13}$					1554.84	2.3		
$f_{11} + f_{16} - f_9$					1647.16	6.0		
$f_9 + f_{16} - f_5$					1719.54	1.7		
$2f_{16} - f_{13}$	1792.59	2.3	1792.26	2.4				
$f_{15} + f_{16} - f_9$	1871.14	2.1						
$2f_{16} - f_9$	1881.22	5.0	1881.58	7.4	1882.58	1.8		
$f_{16} + f_{17} - f_9$					1891.90	3.2		
$2f_{16} - f_6$					1895.53	2.0		
$2f_{16} - f_5$					1968.42	0.8		
$f_{16} + f_{19} - f_9$					2753.84	2.3		
$f_1 + f_{13} + f_{16}$	3830.15	3.2	3830.15	3.0				
$f_1 + f_9 + f_{17}$	3850.16	1.0						
$3f_5$							3901.87	3.8
$2f_5 + f_9$					3982.84	3.7	3986.57	7.7
$f_5 + 2f_9$					4068.67	3.9	4071.26	3.3
$2f_5 + f_{13}$							4074.29	3.9
$f_5 + f_9 + f_{11}$					4082.12	1.6		
$f_1 + 2f_{16}$	4087.98	2.2						
$2f_5 + f_{16}$					4231.71	2.8		
$f_5 + f_9 + f_{16}$					4317.55	6.7		
$f_5 + f_{10} + f_{16}$					4327.62	1.5		
$2f_9 + f_{16}$	4404.35	2.2	4404.85	5.3	4403.38	1.6		
$f_5 + f_{13} + f_{16}$					4405.73	1.5		
$f_9 + f_{12} + f_{16}$	4483.02	0.8						
$2f_5 + f_{18}$							4488.84	2.5
$f_9 + f_{13} + f_{16}$	4492.98	1.6	4494.18	2.3				
$f_5 + 2f_{16}$					4566.42	1.6		
$f_5 + f_9 + f_{18}$					4571.18	2.2	4573.54	3.7
$f_9 + 2f_{16}$	4652.21	4.9	4652.83	5.1	4652.25	2.0		
$f_9 + f_{16} + f_{17}$	4662.25	1.5	4662.19	2.1				
$f_1 + f_9 + f_{19}$	4711.62	0.9						
$f_{13} + 2f_{16}$	4740.83	1.7						
$f_5 + f_{16} + f_{18}$					4820.05	1.5		
$3f_{16}$	4900.07	1.9						
$f_9 + f_{16} + f_{18}$					4905.88	2.0		
$f_{13} + f_{16} + f_{17}$	5473.54	2.6						
$f_9 + f_{16} + f_{19}$			5524.21	1.8				
$f_{16} + f_{17} + f_{19}$	5781.61	1.6						

Table 5. Fourth and fifth-order combination frequencies in our light curves of EC 14012−1446

	April 2004		June 2004		May 2005		April 2007	
ID	Freq. (μHz)	Ampl. (mmag)	Freq. (μHz)	Ampl. (mmag)	Freq. (μHz)	Ampl. (mmag)	Freq. (μHz)	Ampl. (mmag)
$f_9 + f_{16} - 2f_{13}$			69.32	5.5				
$2f_9 - f_5 - f_{11}$					72.38	1.8		
$f_9 + f_{16} - 2f_5$					420.54	2.6		
$2f_{16} - 2f_5$					669.41	1.8		
$2f_{16} - f_4 - f_5$					672.69	2.1		
$f_1 + f_9 + f_{17} - f_{16}$	2216.80	2.1						
$3f_5 - f_{16}$					2263.30	2.7		
$f_4 + f_5 + f_9 - f_{16}$					2345.85	2.2		
$2f_5 + f_9 - f_{16}$					2349.13	3.3		
$f_5 + f_8 + f_9 - f_{16}$					2432.10	2.1		
$f_5 + 2f_9 - f_{16}$					2434.97	2.0		
$2f_5 + f_9 - f_6$							2615.68	3.2
$2f_5 + f_{15} - f_6$							2853.56	3.1
$2f_9 + f_{13} - f_5$					2943.69	2.2		
$f_4 + 2f_{16} - f_9$					3178.31	1.2		
$3f_{16} - f_9$	3514.57	2.7	3515.19	4.3				
$f_1 + 2f_9 + f_{16}$	5225.61	1.7						
$3f_5 + f_9$							5287.19	2.7
$2f_5 + 2f_9$					5367.68	1.8		
$2f_5 + f_9 + f_{16}$					5616.55	2.5		
$f_5 + 2f_9 + f_{16}$					5702.38	1.9		
$3f_9 + f_{16}$	5789.85	1.2						
$f_5 + f_9 + 2f_{16}$					5951.26	1.0		
$f_5 + 2f_9 + f_{18}$					5956.01	1.0		
$2f_9 + 2f_{16}$			6038.46	3.0				
$f_5 + f_9 + f_{16} + f_{18}$					6204.89	1.0		
$3f_{16} + f_9$	6285.57	2.0						
$f_9 + 2f_{13} + f_{16}$	6689.76	1.1						
$f_9 + f_{13} + f_{16} + f_{17}$	6859.04	1.4						
$2f_5 + f_9 - f_{11} - f_{16}$					950.85	2.6		
$3f_9 - f_5 - f_{18}$					968.17	1.8		
$3f_5 + f_9 - f_{16}$					3648.13	2.3		
$f_5 + f_{11} + f_{16} + f_{19} - f_{18}$					4948.63	1.3		
$3f_5 + 2f_9$					6666.68	1.1		
$3f_5 + f_9 + f_{16}$					6915.55	0.8		
$2f_5 + 2f_9 + f_{16}$					7001.39	1.1		

Figure 4 shows the ratio of the amplitudes of the individual combination frequencies with respect to the product of the amplitudes of the parent signals. Note that these amplitude ratios are given in units of mag^{-1}, whereas the amplitudes themselves are quoted in millimagnitudes. Whereas 85% of the data points are located in an interval of 8.5 ± 6.2 mag^{-1}, the remaining combinations show considerably larger amplitude ratios.

By far the largest amplitude ratio is due to the combination frequency at 2196 μHz present in both data sets from the year 2004. It therefore is our best candidate for a resonantly coupled mode. In addition, the second-order combination at 2296 μHz also stands out in Fig. 4. Both of these combinations include the lowest-frequency independent signal $f_1 = 821\,\mu$Hz. This latter signal also has two other combinations with rather large amplitude ratio with respect to its parent variations (at 2207 and 2455 μHz, respectively). The third combination that shows enhanced amplitude in both data sets from 2004 is the one at highest frequency, involving f_{19}. Finally, the combination frequency difference at 268 μHz in June 2004 also has large amplitude, but the residual amplitude spectrum in this data set has high noise around this frequency. We therefore suspect that the large amplitude of the 268 μHz signal may be spurious.

Turning to the data sets from 2005 and 2007, we do not find such extreme amplitude ratios. Three of the five high-amplitude combination frequencies again involve f_{19}, and the other two contain "satellite" frequencies around the strong signal at $f_9 \approx 1385$ μHz. Of highest interest is the combination at 1133.75 μHz in the April 2007 data. Its frequency is consistent within the errors with that of the independent signal f_2 that was only present in the year 2004. However, in 2004 only one of the parents of the combination present in 2007 was detected. Therefore f_2 must be regarded as an independent signal in the data from 2004.

We remind that during the four epochs of observations of EC 14012−1446 at our disposal, amplitude variations occurred. This puts us into a position to examine whether or not the amplitudes of combination signals present in more than one of these data sets followed the corresponding

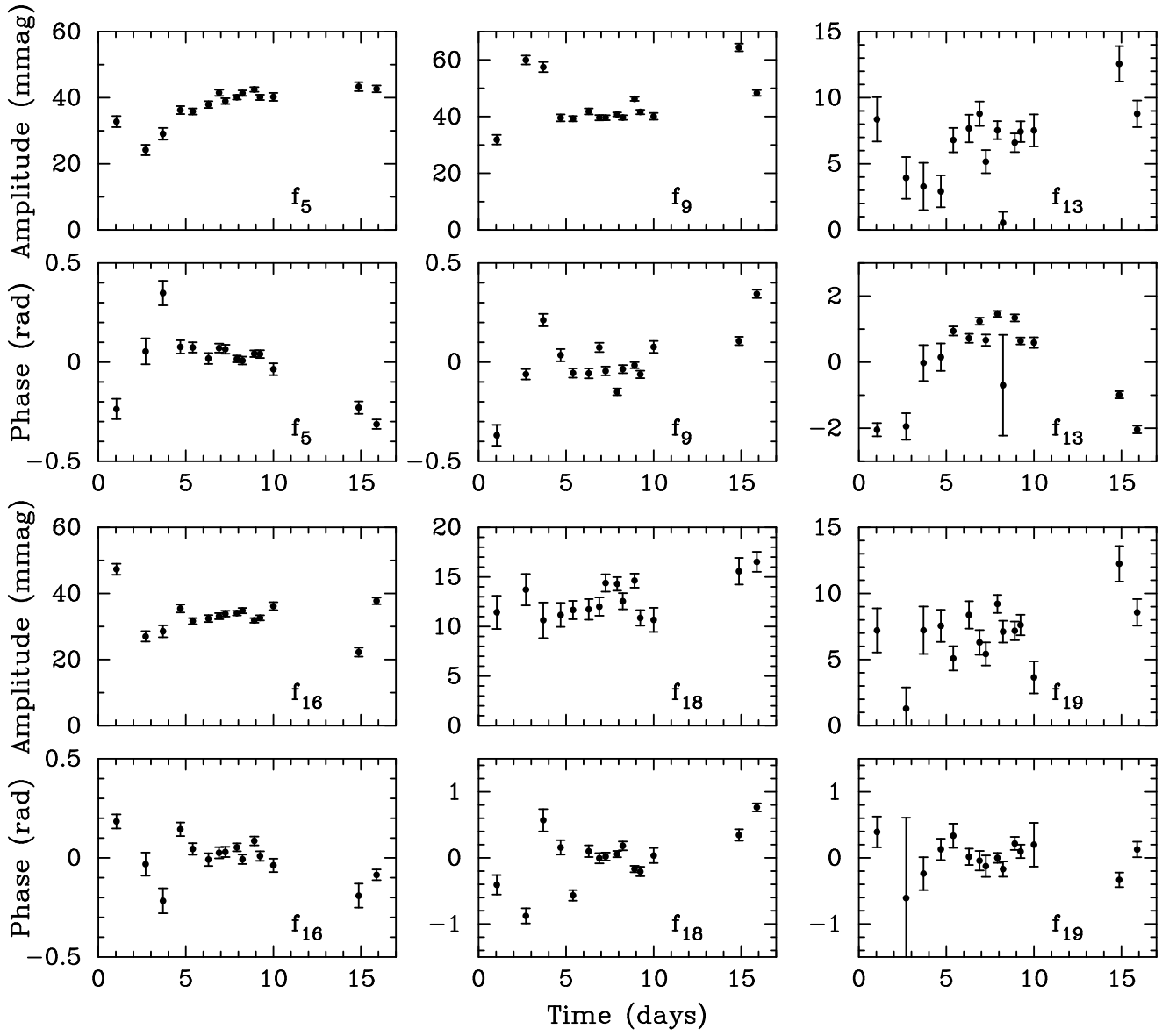

Figure 3. Amplitude and frequency variations of six independent signals in the light curve of EC 14012−1446 during the observations in May 2005. The error bars of the individual data points are 1σ. The panels are grouped with respect to the signal, and have been arranged to compare the amplitude and phase behaviour directly. Note the different ordinate scales in the different panels. The central subset of data used for frequency analysis corresponds to $4 < \mathrm{Time} < 10$ in this graph.

changes of their parent signals. We restrict this analysis to the combination frequency sums because these are less affected by observational noise, i.e. have better signal-to-noise on average.

In order not to make any assumptions about the origin of the combination frequencies, we chose to compare the individual amplitude ratios of the combinations that occur in more than one data set with respect to their mean and their deviations from their formal accuracies. If there were no changes in the relative amplitudes, we would expect a normal distribution to result. The outcome of this test can be found in Fig. 5.

Most of the amplitude ratios follow a Gaussian distribution with a width of $\approx 1.2\sigma$. Given the fact that formal errors of the determinations of amplitudes tend to underestimate the real errors, this is not surprising.

There are nine recurring second-order combination signals whose relative amplitude varies significantly, and they correspond to four different sets of parents: $f_5 + f_9$, $f_6 + f_9$, $2f_9$, and $f_9 + f_{16}$. All these combinations contain the mode f_9, but we failed to find any systematics in the temporal behaviour of the relative amplitudes of its combinations due to the sparsity of data.

We also tested whether possible interactions with other combinations that happen to have frequencies close to the four signals under investigation might be able to affect their amplitudes. The result of this test was negative because in general all possible alternative parent frequency combinations have much lower amplitudes than the parents we assigned. The single exception to this rule is $2f_9$ in the 2007 data set, whose amplitude could be mildly affected by interference with $f_6 + f_{11}$.

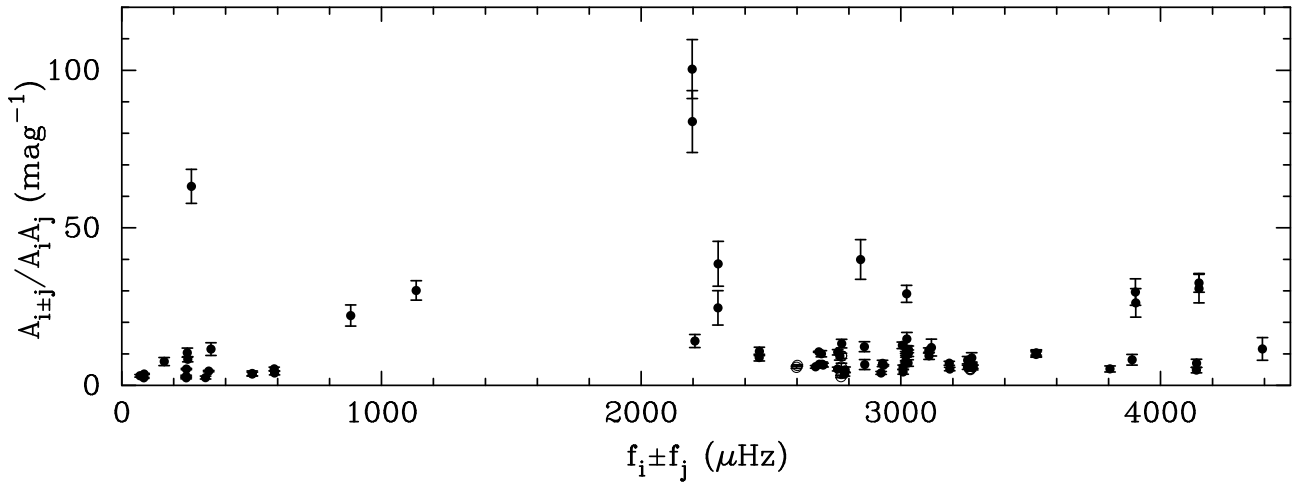

Figure 4. Amplitude ratios between the second-order combination frequencies and the product of their parent signal amplitudes, with 1σ error bars indicated. Multiple determinations at a single frequency are due to combinations present in more than one data set.

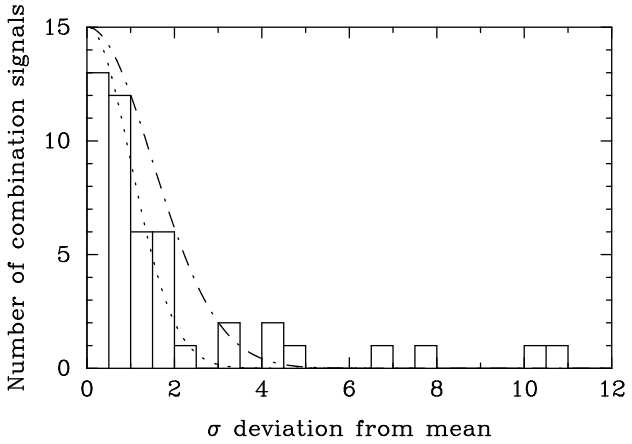

Figure 5. The distribution of the deviation of the amplitude ratios of recurring second-order combination frequencies with respect to their mean and formal errors (histogram bars). For comparison, two Gaussians with standard deviations of 1σ (dotted line) and 1.5σ (dash-dotted line) are shown.

4.3 The third-order combination frequencies

The third-order combination frequencies determined can be separated into two approximately equally populated groups: combinations of the form $f_A + f_B + f_C$ and $f_A + f_B - f_C$, respectively. An important fact about the second type of combination signals it that their frequencies are in the same range as those of the independent signals (see also Vuille et al. 2000). Consequently, they may be mistaken for independent frequencies if not systematically searched for.

As a matter of fact, such confusion has occurred in the preliminary report on EC 14012−1446 by Handler & Romero-Colmenero (2005), where two signals now identified as third-order combination frequencies were believed to be, and interpreted as, independent mode frequencies. We illustrate the severity of this problem in Fig. 6, that shows the schematic amplitude spectrum of our multisite data set with the independent frequencies and combination signals separated. Most of the signals in this frequency range in fact correspond to combination frequencies!

We again stress that we prefer to misinterpret a peak in the amplitude spectrum as a combination signal as opposed to falsely taking combination frequencies as real modes; we followed this guideline throughout the frequency analysis. We will discuss the astrophysical implications of confusing combination signals with independent mode frequencies below.

4.4 The fourth and fifth-order combination frequencies

We were able to identify several high-order combination frequencies in the data. To our knowledge, this is the first report of the detection of fifth-order combination signals in the light curves of a pulsating white dwarf star. The identification of the signals that are pure frequency sums should be secure because there are no ambiguities in assigning the parents, whereas some identifications involving frequency sums and differences may be incorrect. However, it is important to point out that we only matched significant peaks in the amplitude spectrum, and that we succeeded in explaining them all.

5 INTERPRETATION

5.1 The independent frequencies

With our approach to frequency analysis, most of the independent frequencies should correspond to normal mode oscillations. We interpret f_1, f_2, f_{18} and f_{19} as single modes. The triplets f_{12}, f_{13}, f_{14} and f_{15}, f_{16}, f_{17} are normal mode multiplets; their splitting of $\approx 10\,\mu$Hz is most likely due to rotation. We believe that frequency f_9 is also caused a normal mode. It does show a $\approx 10\,\mu$Hz splitting at times, but from time to time a $\approx 14.5\,\mu$Hz splitting is present. The signal f_5 is also suggested to be caused by a normal mode, and it once showed a companion frequency again separated by $\approx 10\,\mu$Hz.

Assuming that the modes where we found rotational splitting have a spherical degree $\ell = 1$, we can estimate the

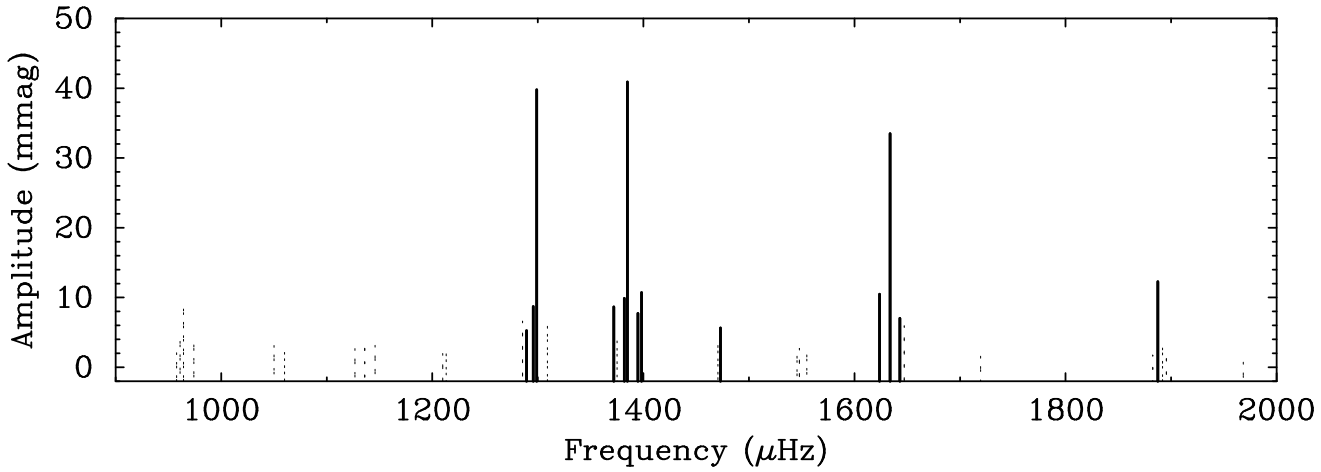

Figure 6. Schematic amplitude spectrum of the May 2005 data (see Tables 2 and 4). The independent frequencies are the thick full lines, whereas the third-order combination frequencies are shown with thin dotted lines.

rotation rate of the star. The average amount of the splitting we believe to be of rotational origin is $9.94 \pm 0.12\,\mu$Hz. Taking into account that this is about 4% off the asymptotic value (Brassard et al. 1992) and that the rotational splitting is somewhat variable, we arrive at a rotation frequency of $19.1 \pm 0.8\,\mu$Hz or at a fairly short rotation period of 0.61 ± 0.03 d.

Some of the independent signals in our light curves (f_4, f_6, f_8, f_{11}) did not conform to rotationally split peaks as interpreted before. There may be two possibilities for their origin. Firstly, they could be members of rotationally split multiplets with different ℓ. However, no reasonable assumption (either the $\approx 10\,\mu$Hz splitting is due to $\ell = 1$ modes or it is due to the $\ell = 2$ rotational splitting) in this framework can explain the whole set of signals detected around f_9. Secondly, these unexplained signals may be artefacts due to amplitude and/or frequency variations. We recall from Sect. 4.1.1 that although such temporal variability in the amplitude spectra is definitely present, we cannot prove this hypothesis. In addition, the presence of a "pure" triplet with a $14.5\,\mu$Hz spacing in April 2007 is hard to explain with amplitude/frequency variability only.

The period spacing between the normal modes of a pulsating white dwarf star serves to obtain its mass if it allows a determination of the asymptotic g-mode period separation. Following the discussion above, we interpret f_1, f_2, f_5, f_9, f_{13}, f_{16}, f_{18} and f_{19} as normal mode frequencies with an azimuthal order $m = 0$, but with different radial overtone k and/or spherical degree ℓ. The assignment of m follows from the multiplet structure around f_9, f_{13} and f_{16} (in case they are $\ell = 1$ modes), but is assumed for the others. However, if wrong, this assumption would not significantly affect any mass determination, because the frequency difference of consecutive radial overtones is significantly larger than the rotational splitting.

In any case, our attempts to establish the asymptotic g-mode period separation of EC 14012−1446 failed. There may be two possible causes: firstly, the effects of mode trapping (e.g. see Brassard et al. 1992) could be so strong that no regular period spacing can be found within the few modes available. Secondly, not all of the modes we adopted may have the same spherical degree ℓ. A comparison of the periods of these eight modes with the ones identified as $\ell = 1$ by Kleinman et al. (1998) in G 29-38 shows good agreement except for f_{18}, assuming the stars are homologous. We conclude that an asteroseismic mass determination for EC 14012−1446 must either await the detection of a more complete set of normal modes or requires systematic matching with a model grid (Metcalfe, Montgomery & Kanaan 2004, Castanheira & Kepler 2008).

Table 6. Changes in the light curves of EC 14012−1446.

Month/Year	WMP (s)	$(\sum(A_i)^2)^{1/2}$ (mmag)	rms scatter (mmag)
June 1994	598.4	66.9	− − −
April 2004	658.9	59.9	48.9
June 2004	663.6	64.9	53.6
May 2005	684.4	72.2	60.3
April 2007	692.0	85.7	71.2

With the independent frequencies and their amplitudes determined, we can compute the weighted mean pulsation period of EC 14012−1446 at the different observing epochs, adopting the definition by Mukadam et al. (2006):

$$\mathrm{WMP} = \frac{\sum(P_i A_i)}{\sum(A_i)}, \quad (1)$$

where WMP is the weighted mean period, the P_i are the periods of the individual pulsation modes and the A_i are their respective amplitudes. We also computed the rms scatter of each individual data point in our light curves and the square root of the total power $(\sum(A_i)^2)^{1/2}$ as indications of the pulsation power of the star. The first measure makes the (justified) assumption that the intrinsic variations in our light curves dominate the measurement noise and it reflects the total variability. The second measure requires knowledge of the independent mode frequencies, but allows a direct comparison with the work by Mukadam et al. (2006).

The results of these calculations are given in Table 6. We also computed the WMP and the square root of the total power from the data by Stobie et al. (1995) for complete-

ness. As these authors quoted nightly amplitudes for their independent frequencies, we adopted the mean of these amplitudes to obtain the WMP and $(\sum(A_i)^2)^{1/2}$ for this observing period.

Table 6 shows a clear trend: the mean period of the variability increased from one observing epoch to the next (a fact that can already be seen by eye in Fig. 2). The total light amplitude increased during our observations, but was at an intermediate level when Stobie et al. (1995) observed the star. As with the apparent frequency changes of some individual modes (Sect. 4.1) we caution against interpreting the change in the WMP as a monotonous trend in time: the gaps between our observing runs were considerably larger than the observing runs themselves. Because we have already found amplitude and frequency changes within one observing run, it is quite possible that the star altered its behaviour on time scales not sampled by us.

If we compare these results with the sample of white dwarfs analysed by Mukadam et al. (2006), we find that EC 14012−1446 is among the highest-amplitude ZZ Ceti stars and that it is located close to the centre of the instability strip, consistent with spectroscopic results (Fontaine et al. 2003, Bergeron et al. 2004). The high amplitudes let us speculate that most pulsation modes are indeed $\ell = 1$, suffering the smallest geometrical cancellation. The temporal variation of the WMP we observed is not unusual compared to other ZZ Ceti stars (Mukadam et al. 2007).

5.2 The second-order combination frequencies

Most of the second-order combination signals have amplitudes that scale with the product of the amplitudes of their parent modes. These are consistent with an interpretation in terms of light-curve distortions. Consequently, we can try to determine some convection parameters with light-curve fitting following Handler, Romero-Colmenero & Montgomery (2002), based on Wu's (2001) analytical expressions for the combination signals' amplitude and phases (also see Yeates et al. 2005).

Using the data from April 2004, assuming all parent modes are $\ell = 1$ and only using the mode triplets, we find a response parameter $2\beta + \gamma = 9.8 \pm 0.3$, convective thermal time $\tau_c = 135 \pm 10\,\mathrm{s}$, and an inclination angle $\theta = 29.5 \pm 1.5^\circ$ (see Wu 2001 for the definitions of these parameters) when fitting the light curve. For 2005 however, no satisfactory fit could be obtained.

As noted before, our best candidate for a resonantly coupled mode is the 2196 μHz signal in the 2004 data, as its relative amplitude is by far the highest, and since it varied in accordance with the amplitudes of its parents f_1 and f_7. However, the interpretation of this 2196 μHz signal may be a chicken-and-egg problem: in June 2004, this signal had about 70 per cent of the amplitude of its parent mode f_1. Given that this number is close to unity and that different spherical degrees, and thus different geometrical cancellation, of the parent and the combination frequencies, may come into play, some doubt as to which signal is indeed the parent and which one is the combination remains. In addition, a 2196 μHz signal fits much better into the sequence of the observed mode frequencies of EC 14012−1446 than $f_1 = 821\,\mu$Hz does.

5.3 The third-order combination frequencies

The large number of third-order combination frequencies depicted in Fig. 6 follows a simple structure: all these groups of peaks are separated from the dominant modes by the frequency differences between the three strongest modes and their rotationally split components. This means we see a pattern fairly regularly spaced in frequency, which, to first order, is also a pattern regularly spaced in period.

If those third-order combinations are not correctly identified, but are misinterpreted as independent frequencies, an incorrect determination of the period spacing of the normal modes may therefore result. As an experiment, we determined the mean period spacing of all independent and third-order combination frequencies detected between 950 and 2550 μHz in the May 2005 data. We arrived at a formally significant mean period spacing of 17.7 s. Some "radial overtones" in this scenario would be missing, but no integer multiple of 17.7 s would give a reasonable fit. Incidentally, this completely incorrect period spacing is close to the true period spacing of the massive ZZ Ceti star BPM 37093 (Kanaan et al. 2005). Hence, EC 14012−1446 could be misinterpreted as having high mass, inconsistent with spectroscopic results (Fontaine et al. 2003). It is therefore essential that combination frequencies are correctly recognized in the amplitude spectra of pulsating white dwarf stars.

Vuille et al. (2000) pointed out a similar problem in their study of the prototype pulsating DB white dwarf star GD 358. However, there are some differences between our results and those by Vuille et al. (2000): the third-order combination frequencies revealed in their work only manifested themselves as "odd" peaks lying close to or within rotationally split multiplets, and these authors could explain all of these "odd" peaks with combination frequencies. In our case, the third-order combinations create apparent additional frequency multiplets, and we found signals within the rotationally split normal mode multiplets that we were unable to explain by combination frequencies; we suspect they are artefacts caused by amplitude/frequency variations during the measurements.

6 CONCLUSIONS

We have acquired more than 200 hours of time-resolved photometry of the ZZ Ceti star EC 14012−1446. The star turned out to have a complex pulsation spectrum, that we were able to understand to some extent, but not to our full satisfaction.

We detected eight normal modes of the star with different radial overtones. Not all of them must necessarily have the same spherical degree ℓ. Some of the normal modes are arranged in groups, in most cases showing separations of $\approx 10\,\mu$Hz. We interpreted that as the sign of rotational m-mode splitting, and inferred the rotation period of the star ($0.61 \pm 0.03\,\mathrm{d}$), assuming modes of $\ell = 1$.

We were unable to determine a regular period spacing between the pulsation modes of EC 14012−1446, and therefore cannot provide a mass estimate. The reason may be mode trapping or that we see a mixture of modes with different spherical degree ℓ.

The pulsation spectrum of the star changes over time.

We have measured changes of ±8% in the weighted mean period and of ±20% in the square root of the total pulsation power. Our data have insufficient sampling and time base to determine the time scale of the variations in the normal modes. However, we found systematics in the temporal changes of the pulsation spectrum: the higher the radial overtone of a mode, the more pronounced the variations are and amplitude and frequency changes go hand in hand. The dependence on radial overtone is easy to understand: since the kinetic energy of the g modes in a pulsating white dwarf star becomes weighted towards the outer regions with increasing radial overtone, less energy is required to disturb a high-overtone mode.

Most of the second-order combination frequencies have amplitudes consistent with the hypothesis that they originate from light curve distortions of the star. However, some could be resonantly excited modes because they have relative amplitudes much higher than the other second-order combinations. We even found one case where it was no longer clear which was the parent mode and which was the combination, although this could partly be an effect of geometrical cancellation.

The amplitudes of the second-order combinations varied in time in accordance with their parent modes. The exceptions to this rule are a number of combinations that involve the mode f_9. This mode is also special in the sense that it shows complicated "multiplet" structure in one of our data sets, that we tentatively attributed to the effects of amplitude and frequency variations during the observations.

Finally, we showed how a misinterpretation of third-order combination frequencies of the form $f_A + f_B - f_C$ as normal modes, can lead to a completely nonsensical determination of the stellar mass. Combination frequencies intruding into the domain of the normal modes in the Fourier spectra of the light curves must be carefully searched for, and eliminated from an asteroseismic analysis.

The ZZ Ceti star EC 14012−1446 remains an attractive target for further study, as we could only partly understand its pulsations. The high pulsation amplitudes of the star may facilitate the application of Montgomery's (2005) method to determine convection parameters and mode identifications from high signal-to-noise light curves. The detection of more normal modes of pulsation and the correct identifications of at least some of them may permit a full asteroseismic analysis. A reliable determination of the time scales of the amplitude and frequency variations of the star would be worthwhile to pin down their origin, but would require a data set with a time base in excess of two weeks, excellent duty cycle at the same time, as well as a co-operating target. Under such circumstances, precision asteroseismology of a ZZ Ceti star may be feasible.

ACKNOWLEDGEMENTS

This work has been supported by the Austrian Fonds zur Förderung der wissenschaftlichen Forschung under grant P18339-N08, Mt. Cuba Observatory and the Delaware Asteroseismic Research Center. This material is based upon work supported by the National Science Foundation under Grant No. AST 0205902 to the Florida Institute of Technology. GH thanks Barbara Castanheira Endl and Victoria Antoci for commenting on a draft version of this paper.

This paper has been typeset from a TEX/ LATEX file prepared by the author.

REFERENCES

Bergeron P., Fontaine G., Billères M., Boudreault S., Green E. M., 2004, ApJ, 600, 404
Brassard P., Fontaine G., Wesemael F., Tassoul M., 1992, ApJS, 81, 747
Breger M. et al., 1993, A&A, 271, 482
Breger M. et al., 1999, A&A, 349, 225
Brickhill A. J., 1992, MNRAS, 259, 519
Castanheira B. G. et al., 2004, A&A, 413, 623
Castanheira B. G. et al., 2007, A&A, 462, 989
Castanheira B. G., Kepler S. O., 2008, MNRAS, in press
Dziembowski W. A., 1982, Acta Astr., 32, 147
Fontaine G., Brassard P., Bergeron P., 2001, PASP, 782, 409
Fontaine G., Bergeron P., Billères M., Charpinet S., 2003, ApJ, 591, 1184
Handler G., Romero-Colmenero E., 2005, in Koester D., Moehler S., eds, *14th European Workshop on White Dwarfs*, ASP Conf. Ser. Vol. 334, p. 569
Handler G., Romero-Colmenero E., Montgomery M. H., 2002, MNRAS, 335, 399
Handler G. et al., 2003, MNRAS, 340, 1031
Hansen B. M. S. et al., 2007, ApJ, 671, 380
Kanaan A., Kepler S. O., Winget D. E., 2002, A&A, 389, 896
Kanaan A. et al., 2005, A&A, 432, 219
Kepler S. O. et al., 2005, ApJ, 634, 1311
Kjeldsen H., Frandsen S., 1992, PASP, 104, 413
Kleinman S. J. et al., 1998, ApJ, 495, 424
Loumos G., Deeming T. J., 1978, Ap&SS, 56, 285
Metcalfe T. S., Montgomery M. H., Kanaan A., 2004, ApJ, 605, L133
Montgomery M. H., 2005, ApJ, 633, 1142
Montgomery M. H., Winget D. E., 1999, ApJ, 526, 976
Mukadam A. S., Winget D. E., von Hippel T., Montgomery M. H., Kepler S. O., Costa A. F. M., 2004, ApJ, 612, 1052
Mukadam A. S., Montgomery M. H., Winget D. E., Kepler S. O., Clemens J. C., 2006, ApJ, 640, 956
Mukadam A. S., Montgomery M. H., Kim A., Winget D. E., Kepler S. O., Clemens J. C., 2007, in Napiwotzki R., Burleigh M. R., eds, *15th European Workshop on White Dwarfs*, ASP Conf. Ser. Vol. 372, p. 587
O'Donoghue D., 1995, Baltic Astronomy, 4, 519
Pech D., Vauclair G., Dolez N., 2006, A&A, 446, 223
Richer H. B., Hansen B., Limongi M., Chieffi A., Straniero O., Fahlman G. G., 2000, ApJ, 529, 318
Stobie R. S., O'Donoghue D., Ashley R., Koen C., Chen A., Kilkenny D., 1995, MNRAS, 272, L21
Vuille F., et al., 2000, MNRAS, 314, 689
Winget D. E., Hansen C. J., Liebert J., van Horn H. M., Fontaine G., Nather R. E., Kepler S. O., Lamb D. Q., 1987, ApJ, 315, L77
Winget D. E. et al., 1991, ApJ, 378, 326
Winget D. E. et al., 1994, ApJ, 430, 839
Wu Y., 2001, MNRAS, 323, 248
Yeates C. M., Clemens J. C., Thompson S. E., Mullally F., 2005, ApJ 635, 1239